Available online at www.sciencedirect.com
ScienceDirect
International Journal of Heat and Fluid Flow 29 (2008) 340–351
International Journal of HEAT AND FLUID FLOW
www.elsevier.com/locate/ijhff

Horseshoe vortex studies in the passage of a model plate-fin-and-tube heat exchanger

Besir Sahin [a,*], Nurhan Adil Ozturk [b], Cahit Gurlek [a]

[a] Cukurova University, Faculty of Engineering and Architecture, Department of Mechanical Engineering, 01330 Adana, Turkey
[b] Mustafa Kemal University, Faculty of Engineering and Architecture, Department of Mechanical Engineering, 01330, Adana, Turkey

Received 7 June 2006; received in revised form 15 June 2007; accepted 18 June 2007
Available online 27 July 2007

Abstract

An experimental investigation is reported using particle image velocimetry of the flow structure in the flow through a rectangular duct containing a circular cylinder with axis normal to the flow. A duct with a narrow gap was designed to simulate a fin-tube heat exchanger containing a single circular cylinder. The time-averaged velocity vectors map, $\langle V \rangle$, patterns of streamlines, $\langle \psi \rangle$ and corresponding vorticity contours, $\langle \omega \rangle$ were obtained using 490 instantaneous images. Development of the entrainment process between the main flow and wake-flow regions is magnified by a helical horseshoe vortex system emerging upstream of the cylinder. The occurrence and development of boundary layer separation and the formation of horseshoe vortices upstream of the cylinder close to both upper and lower plate surfaces and the merging of these developing horseshoe vortices into a primary horseshoe vortex system were also observed in the side-view plane for the Reynolds number range of $1500 \leqslant Re_d \leqslant 6150$.

Keywords: Horseshoe vortex; Fin-tube heat exchanger; PIV; Wake flow; Confined flow

1. Introduction

Heat transfer in heat exchangers is strongly related to the flow structure. Plate-fin-and-tube heat exchangers are commonly used in space heating and/or cooling devices such as air-conditioning systems, fan-coils and radiators, in condensers and evaporators, and in heat recovery systems. Manufacturers mostly prefer plain fin among the wavy, slit and louvered fin configurations due to the long term operation and simplicity. Sheui et al. (1999) numerically studied the heat transfer in two-row tube heat exchangers having slotted fins and laminar flow. In general, these fins can be divided into louvered, radial-strip, parallel-strip and wavy-strip types. In this type of geometry, the physical complexity comes from the three-dimensional boundary layer development and the subsequent flow separation. Their study revealed that the three-dimensional vortical flow structure becomes more energetic because of the perforated fin surface leading to an increase in the heat transfer rate but causing further pressure losses. Umeda and Yang (1999) applied a tracer injection method to visualize streamlines, and both piezometry and two-dimensional laser-Doppler velocimetry (LDV) were used for flow measurement through the staggered tube bundles. Their main findings were: (i) the shape and dimension of a wake vortex formed behind the tube depended upon the staggered arrangement angle and the Reynolds number, and (ii) flow conditions around the tube varied with the staggered arrangement angle. The Von Karman vortex street oscillation induced a flip-flop flow having a staggered angle of 30°. A symmetric flow formed and the wake vortex was confined when the staggered angle of the tube bundles was set to 60°. Tutar and Akkoca (2004) studied numerically the time evolution of a horseshoe vortex system and the details of flow structure affecting the heat transfer coefficient in the base of the circular cylinder in between two

* Corresponding author. Tel.: +90 322 3387063; fax: +90 322 3386126.
E-mail address: bsahin@cu.edu.tr (B. Sahin).

0142-727X/$ - see front matter © 2007 Elsevier Inc. All rights reserved.
doi:10.1016/j.ijheatfluidflow.2007.06.005

closely fixed parallel plates. A numerical investigation of flow structure and heat transfer rate in a rectangular duct with a built-in circular tube was performed by Tiwari et al. (2003) for moderate Reynolds numbers and varying blockage ratios. The duct was designed to simulate a passage formed by two neighboring fins in a fin-tube heat exchanger. Close to the tube in a narrow duct a screw-like motion of a helical vortex tube occurs. The rate of heat transfer is increased by inducing swirling motion in the wake region, as pointed out in the studies which were experimentally conducted by Sumner et al. (1997) and numerically performed by Yuhi et al. (1999). A three-dimensional numerical study was also conducted by Tsai and Sheu (1998) in order to examine the flow structure and performance of conjugate heat transfer in a finned-tube heat exchanger element. The physical domain they considered comprised a double row of staggered cylinder tubes which were normal to two packed plane plates. For the calculation of heat transfer between the gaseous and solid phases, the complex flow structure was considered as three-dimensional, thermally and hydrodynamically developing laminar flow. It was found that the rate of heat transfer increased due to the presence of helical horseshoe vortices which formed in the upstream base of the tube close to the lower and upper fin plates and wrapped around the tube. Spiraling motion of horseshoe vortices adjacent to their central lines creates an exchange of fluid between the main and wake-flow regions. Tsai and Sheu (1998) also indicated that due to the geometrical complexity of finned-tube heat exchangers, for example, reducing the space between two adjacent fins causes experimental difficulties. For these types of practical reasons, the extensive efforts have been devoted to numerical investigations.

Roulund et al. (2005) performed numerical and experimental work on the flow around a vertical circular pile exposed to a steady flow. They basically studied the effect of boundary-layer thickness, Reynolds number and bed roughness on the horseshoe vortex system. Their numerical results show that the horseshoe vortex disappears when the boundary-layer thickness to pile diameter ratio δ/d is less than $\delta/d < 0.01$ for $Re_d = 2 \times 10^5$. The influence of the Reynolds number, Re_d on the size of the horseshoe vortex is significant. In laminar flow, the size of the horseshoe vortex and the bed shear stress increase with increasing Reynolds number; on the other hand, the opposite changes take place in the turbulent regime. An extensive review by Sarpkaya (2004) covers the fundamental aspects of bluff body flows, in particular flows past a circular cylinder. Kirkil et al. (2005) concluded that the structure of the horseshoe vortex system is very organized and periodic when the incoming boundary-layer is laminar. But, the horseshoe vortex system has a wide range of a coherent structure with a wide range of energetic frequencies in the velocity and pressure spectra when the approaching flow is turbulent. A review by Simpson (2001) reports various physical features of junction flows around bluff bodies. He discussed the fact that horseshoe vortices form in all types of bluff body junctions causing high turbulence intensities, pressure fluctuations, heat transfer rates and a scouring around the obstacle's base. The cylinder induces a strong distortion on the spatial development of the mixing layer. Lin et al. (2002) investigated a horseshoe vortex system near the juncture of a vertical plate normal to the flow direction using flow visualization, fiber laser-Doppler velocimetry and particle image velocimetry (PIV) systems. The PIV technique in the region close to the vertical cylinder and base plates was successfully applied to study horseshoe vortex formations that cannot be achieved using more traditional tools. Velocity vectors obtained by PIV and corresponding streamline patterns indicate that there are several concentrated vortices in the boundary-layer region above the base plate surface. These vortices correspond exactly to those seen by the flow visualization technique. Akilli and Rockwell (2002) and Fu and Rockwell (2005) investigated experimentally the horseshoe vortex system and wake-flow regions around a vertical cylinder mounted on a flat plate in shallow-water flow, examining the development of horseshoe vortex systems and the convection of these vortices further downstream which interact with shedding vortices close to the base plate surface. The main findings of Fu and Rockwell (2005) are: (i) the instability of the horseshoe vortices emerging upstream of the vertical cylinders activates the instability of flow in the near wake, (ii) increasing the fluctuation level in the horseshoe vortices causes the development of coherent vortical structures earlier in the separating shear layer, and (iii) rotational perturbation of a vertical cylinder can destabilize the wake-flow structure.

In the literature, there are a number of numerical studies on the performance, geometrical parameters, flow properties, and heat transfer characteristics of compact heat exchangers. Among them, Wung and Chen (1989) predicted the heat transfer and flow data and found that the heat transfer tended to peak in the upstream surface of the cylinder, and became a minimum in the wake-flow region. Beale and Spalding (1999) used a version of the SIMPLE algorithm and the PHOENICS computer code to present the time-averaged and unsteady flow and temperature distributions around an in-line and a staggered tube bank. Similarly, Tsai et al. (1999), Tsai and Sheu (1998), Rocha et al. (1997), Barsamian and Hassan (1997), Jang et al. (1996), Jang and Chen (1997), and Kundu et al. (1992) performed numerical calculations or simulations to investigate the flow structure and heat transfer characteristics of these types of heat exchangers with various geometrical configurations. There are also a number of experimental studies regarding flow properties, heat-transfer characteristics, and the horseshoe vortex system formed in the passage of heat exchangers with built-in cylinders. Saboya and Sparrow (1974), Goldstein and Sparrow (1976), Rocha et al. (1997), and Kim and Song (2002, 2003) used the naphthalene sublimation technique to measure local heat and mass transfer coefficients on the fin surface and examined a main and a subsidiary horseshoe

vortex causing a substantial increase in total heat and mass transfer rates in front of the cylinders, but low heat and mass transfer coefficients in the wake region downstream of the cylinders. Authors suggested an optimal non-dimensional length between the two cylinder centers as $h/d = 0.5$ where h is the distance between the two parallel plates and d is the diameter of the cylinder, considering the high heat transfer rates and minimum pressure drops.

The numerical study of Akkoca (2004) and experimental and numerical studies of Mendez et al. (2000) reported that no horseshoe vortices appear in the fin and tube junction for the Reynolds number range $1200 \leqslant Re_d \leqslant 1460$ having fin spacing of $0.116 \leqslant h/d \leqslant 0.265$. They also indicated that horseshoe vortices in the fin and cylinder junction having $h/d = 0.365$ and $Re = 1460$ were present. Kim and Song (2002) concluded that the subsidiary horseshoe vortex was formed when Re_d was increased to about 2660 for $h/d = 0.2$. The three-dimensional numerical studies of Torikoshi et al. (1994) revealed that as the fin spacing increases the flow structure is destabilized which enhances the heat transfer rate. Numerical studies of Khallaki et al. (2005) indicated that the horseshoe vortex structure upstream of a single plate-finned-tube heat exchanger is altered substantially when varying the fin spacing from $h/d = 0.13$ to $h/d = 0.27$ and the Reynolds numbers from $Re_d = 2260$ to $Re_d = 3800$. Akkoca (2004) clearly showed that as the fin spacing is increased there is a sharp increase in the average heat transfer coefficient for $h/d < 0.15$ and finally that this heat transfer coefficient becomes constant for $0.25 \leqslant h/d \leqslant 0.5$ and $Re_d = 920$. Secondly, as the fin spacing increases the value of pressure drop coefficient decreases for h/d up to 0.35 and, finally, the pressure drop coefficient is constant for $h/d > 0.35$. Consequently, the optimum fin spacing should correspond to a minimum pressure drop, but, a maximum heat transfer. Finally, for this reason, in the present study, the value of the fin spacing, h/d is taken as 0.4.

In the present work, a single circular cylinder was fixed between parallel flat plates for a height-to-cylinder diameter ratio of $h/d = 0.4$. Sahin et al. (2006) investigated the flow characteristics in a plate-fin-and-tube heat exchanger model composed of a single cylinder, using particle image velocimetry (PIV). A similar geometry and flow conditions were used in the present work in order to gain further information about the development of the horseshoe vortex system upstream of the base of the cylinder, the entrainment process and the circulatory motion along the shear layers which are magnified by emerging horseshoe vortices. In the present work, a small area of the flow field was experimentally examined comparing to the work of Sahin et al. (2006) in order to see the boundary-layer separation process, the formation of horseshoe vortices, the wake and shear flow interaction under the influence of horseshoe vortices in detail. The time-averaged and instantaneous values of velocity vectors, streamlines and corresponding vorticity were studied in the flow passage close to the lower plate surface and across the central axis on horizontal and vertical planes.

2. Experimental set-up and instrumentations

Experiments were conducted in a circulating free-surface water channel. The internal dimensions of the water channel are of 8000 mm × 1000 mm × 750 mm which is made from 15 mm thick transparent plexiglass sheet. Before reaching the test chamber, the water was pumped into a settling chamber and passed through a honeycomb section and a 2:1 channel contraction. The depth of the water in the test section was adjusted to 600 mm height for the present experiments. The water pump was driven by an electric motor with a variable speed controller. A schematic of the test chamber of rectangular duct with built-in cylinder is shown in Fig. 1. The test section consists of a circular cylinder 50 mm in diameter attached to the lower plate and mechanically press fitted to the upper plate which is placed in an open water channel flow. The test chamber and cylinder are made of plexiglas material so that laser light propagates easily from the plates and cylinder. The distance between the upper and lower plates is $h = 20$ mm. The ratio of the rectangular duct height to the diameter of the circular cylinder is $h/d = 0.4$ which is sufficient for the formation of horseshoe vortices which enhance the heat transfer rate. To avoid flow disturbances that may occur in the test chamber, the leading edges of the plates are specially beveled. The lengths of the plates extend 20 times the cylinder diameter in the longitudinal and 14 times in the transverse directions. The distance between the centre of the cylinder and the leading edge of the flat plate is $10d$ or $25h$ and the downstream length between the center of the cylinder and the trailing edge of the flat plate is $10d$ or $25h$.

The PIV technique is capable of studying unsteady and wake-flow phenomena by the scanning technique over a certain area of the flow field with a high level of accuracy. PIV imaging plan and side-view planes are indicated in Fig. 1. Average free-stream velocities in the side-view planes are $U_{av} = 30$ mm/s, $U_{av} = 80$ mm/s, and $U_{av} = 123$ mm/s, which correspond to Reynolds numbers $Re_d = 1500$, $Re_d = 4000$ and $Re_d = 6150$ based on the cylinder diameter (alternatively $Re_h = 600$, 1600 and 2460 based on the height of rectangular duct and average free-stream velocity, U_{av}). The corresponding Reynolds numbers based on the hydraulic diameter of the rectangular duct are $Re_{hd} = 584$, 1556 and 2400, respectively. According to Re_h and Re_{hd}, the approaching flow for $Re_d = 1500$ and 4000 are laminar.

The instantaneous velocity field in the specified flow passage was measured and the data was recorded using a DANTEC PIV system and Flow Manager Software. The measuring cross-section was illuminated by using a pair of double-pulsed Nd: YAG laser sources of a wavelength of 532 nm, each with a maximum energy output of 120 mJ/pulse. Each laser produced a thin and intensified green light sheet with 1.5 mm thickness. The water flow was seeded with 12 μm metallic coated hollow plastic spheres. Since these particles had the same density as water they were neutrally buoyant. The velocity vector analysis

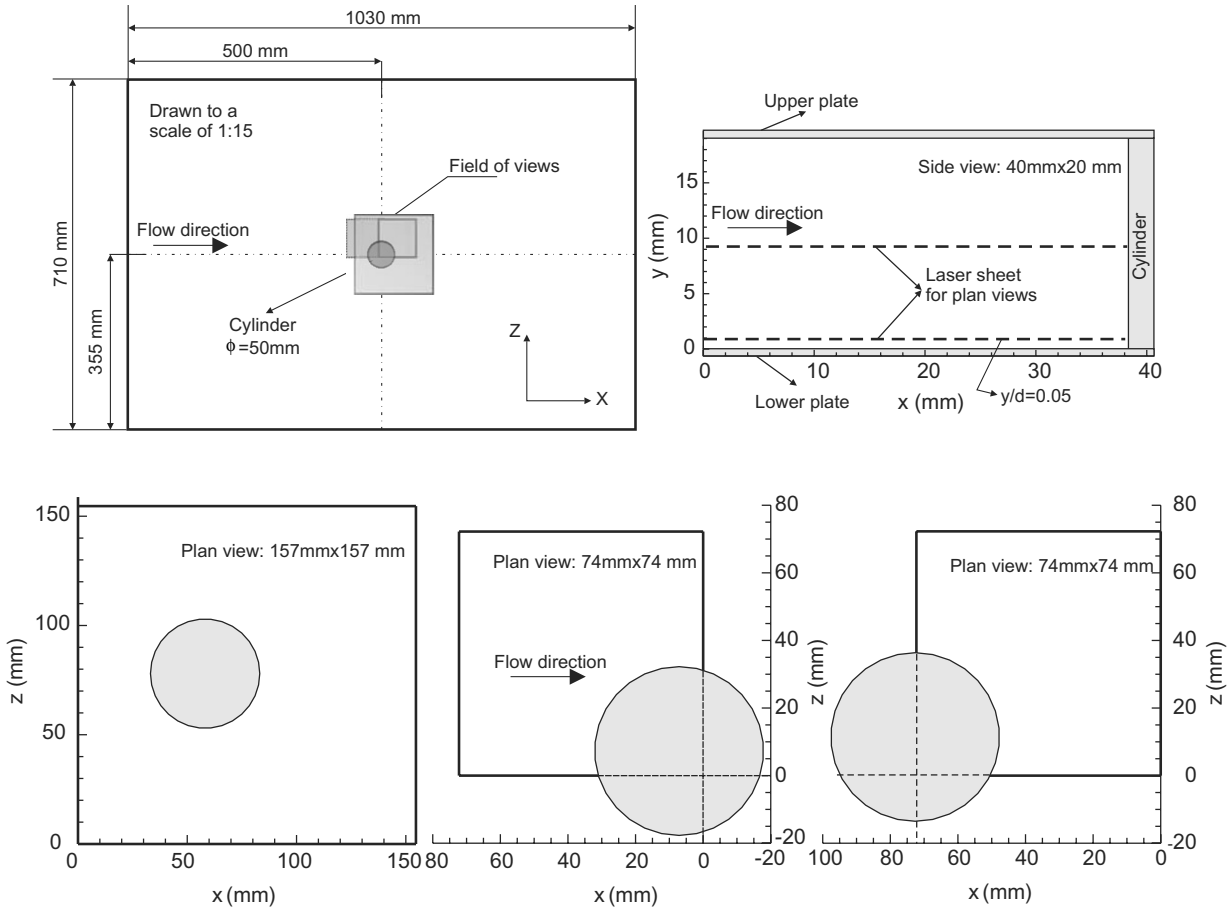

Fig. 1. Schematic of orientation of imaging views and laser sheet.

was performed by recording the locations of the particles throughout the two-dimensional area of the flow field and obtaining the change in position of the particles during the specified time interval between two pulses. A cross-correlation CCD camera with a resolution of 1024×1024 pixels was used to capture the particle images. The camera was equipped with a lens of focal lengths 60 mm and 105 mm. An input buffer was used to read and store the image maps from the CCD camera. To transfer the images from the camera to the computer, a high speed digital frame grabber was employed. To capture the flow field images, the laser pulse and camera must be triggered with the correct sequence and timing. Therefore, a synchronizer was used to control all of the components which were initiated at the exact moment necessary. These captured images were recorded in the computer's memory. A total of 490 instantaneous velocity vector fields were recorded with an acquisition frequency of 10 Hz for each continuous run. The size of the interrogation window was 32×32 pixels with 50% overlap providing 3844 (62×62) velocity vectors over the entire field-of-view plane. The dimensions of the side and plan-view planes shown in Fig. 1 are 157 mm × 157 mm, 74 mm × 74 mm, and 40 mm × 20 mm, respectively.

Dantec flow grabber PIV software employing the frame-to-frame cross- correlation technique was used to calculate the row displacement vectors. The row velocity vector field was determined from this displacement vector field using the time interval between laser pulses. Then, the spurious velocity vectors were detected, using the local median-filter technique (Westerweel, 1994) and replaced by interpolated vectors calculated using a bilinear least-square-fit technique between neighboring vectors.

The PIV technique used during the experiment is similar to that employed by Westerweel (1993) who concluded that the uncertainty in velocity is less than ±2%. Seal et al. (1997) also estimated the uncertainty on the symmetry plane of filmed-based PIV data as ±2%. Comparisons of the time-averaged velocity profile in deep-water flow measured by the present PIV system with the PIV results of Kahraman (2002) and the LDA results of Kirkgoz and Ardiclioglu (1997) showed that the disagreement between the present and these previous results was less than ±2%.

3. Results and discussions

Experimental investigations of the flow structure in the passage of finned-tube heat exchanger are restricted because of the geometrical complexity. Fin configurations are usually plain, corrugated, punched and slotted types. Over the past years, slotted fins have received an increasing

amount of attention in industrial applications. Understanding the flow structures in the heat exchanger flow passage is of substantial importance for the design and optimization purposes. Flow structures in separated flows or wake flows are extremely unsteady. Consequently, flows of this type require spatial and temporal information of the entire flow fields to allow a quantitative detection of spatial structures in unsteady flows as it is not possible with a single measuring technique. With this in mind, laser-based particle image velocimetry was employed. The time-averaged velocity vector map, $\langle V \rangle$, patterns of streamlines, $\langle \psi \rangle$ and corresponding vorticity, $\langle \omega \rangle$ captured in the forward face of the cylinder at an elevations of $y/h = 0.05$ above the lower plate surface and $y/h = 0.5$ at the central plane of the rectangular duct are presented in Fig. 2. The first row of images presents the data of time-averaged flow data at an elevation of $y/h = 0.5$ detecting no horseshoe vortex system and so no saddle points, S appear further upstream of the cylinder. In contrast the remaining images in Fig. 2, taken at an elevation of $y/h = 0.05$ close to the lower plate, show the formation of the horseshoe vortices. It is worth mentioning that, in most cases fin-tube heat exchangers similar to the present rectangular duct geometry with a narrow gap are used. The optimum fin spacing should correspond to the minimum pressure drop, but, maximum heat transfer as Akkoca (2004) suggested. As seen in the second row of images of Fig. 2, the location of the saddle point, S due to the primary rotating horseshoe vortex system appears upstream of the cylinder base at a distance of $L_s = 0.35d$ for $Re_d = 1500$ (and $Re_h = 600$ based on the fin spacing, h). Here, L_s denotes the distance between the location of the saddle point, S and the upstream face of the vertical cylinder. It is worth indicating that for a cylinder with the same diameter in deep-water flow the location of the saddle point, S occurs further upstream at $L_s = 0.72d$ although the incoming flow is turbulent, having a Reynolds numbers of $Re_d = 1500$ and $Re_{hd} = 32{,}730$ based on the hydraulic diameter of the open channel flow (Ozturk, 2006). Increasing the Reynolds number to a value of $Re_d = 6150$, the saddle point, S gets closer to the surface of the cylinder with a distance of $L_s = 0.19d$ as shown in the last row of Fig. 2. On the other hand, Ozturk (2006) reported that this distance, L_s in the case of Reynolds numbers, for $Re_d = 9600$ and $Re_{hd} = 2.1 \times 10^5$ for deep-water flow studies is $L_s = 0.26d$, although the range of the Reynolds number of incoming flow in that study is very high compared to those of the present flow geometry. It can be concluded that the saddle point of the time-averaged flow data appears further upstream for deep-water flow cases compared with the present work. Averaging the instantaneous flow data in the plan-view plane at an elevation of $y/h = 0.05$ eliminates the arbitrarily rotating developing vortices leaving simply the primary vortices. These primary vortices obtained from the time-averaged flow data revolve faster with a high rate of momentum and come closer to the juncture region when the Reynolds number is increased to a value of $Re_d = 6150$ ($Re_h = 2460$). Here, the cluster of focus, the location of the saddle point and the node of attachment and line of coalescence are identified as F, S, N_a and L_c, respectively. A pattern of negative vorticity is indicated with a dashed line and positive vorticity is indicated with a solid line. In the last column of Fig. 2, time-averaged vorticity contours, $\langle \omega \rangle$ are presented. Here, negative and positive vorticity indicate the existence of the horseshoe vortex system convecting downstream along the shear layers.

Fig. 3 presents time-averaged flow data for a flow field imaging dimension of 157 mm × 157 mm in order to capture the flow structure around the cylinder in a complete frame. The first two images show the flow data at an elevation of $y/h = 0.5$ on the central plane. Two foci, F_1 and F_2 occur between the cylinder surface and the saddle point, S. Here, the time-averaged velocity vector map, $\langle V \rangle$ and the pattern of streamlines, $\langle \psi \rangle$ show that flow recirculation only occurs in the wake-flow region, indicating that a low level of entrainment exists between the main flow region and the wake flow. On the other hand, close to the lower plate surface; foci, F_1 and F_2 are developed in between the saddle points, S_1 and S_2 showing that interactions between the shear layers and the horseshoe vortex system stimulate circulatory motion so that a high rate of fresh flow from the main core flow region is entrained into the wake-flow regions; for example, the velocity vector distributions, $\langle V \rangle$ and the pattern of streamlines, $\langle \psi \rangle$ in the last row of images of Fig. 4 clearly reveal this entrainment process which enhances the heat transfer rate in the case of fin-tube heat exchangers. Saddle points, S_1 and S_2 are connected by upstream-oriented streamlines. These streamline patterns leading to the foci, F_1 and F_2 have a spiral nature which indicates that the flow structure near the flat plate surface is three dimensional.

Fig. 4 presents the time-averaged flow data covering the flow field on the left-hand side of the cylinder in the plan-view plane at elevations of $y/h = 0.05$ and 0.5. The first row of images present the time-averaged flow data at an elevation of $y/h = 0.5$, in terms of the velocity vectors map, $\langle V \rangle$, the streamlines, $\langle \psi \rangle$ and the corresponding contours of vorticity, $\langle \omega \rangle$ which presents the boundary of the wake-flow region with a focus F in it. This focus simply rotates between the inner wall of the shear layer and the central axis of the wake region. The rest of the images present the time-averaged flow structures close to the lower plate surface downstream of the cylinder as a function of Reynolds number. For $Re_d = 1500$ the center of the focus is out of the flow field frame. The flow structure for $Re_d = 1500$, reveals that the wake-flow region is larger than for the higher Reynolds number. Along the shear layer, shown by the vorticity contours, a pair of horseshoe vortices appears and moves further downstream. The flow structure for $Re_d = 4000$ and 6150 presented in the third and fourth rows of Fig. 4 demonstrates that the mixing process takes place between core and wake-flow regions. Constantinescu and Koken (2005) stated that the horseshoe vortex

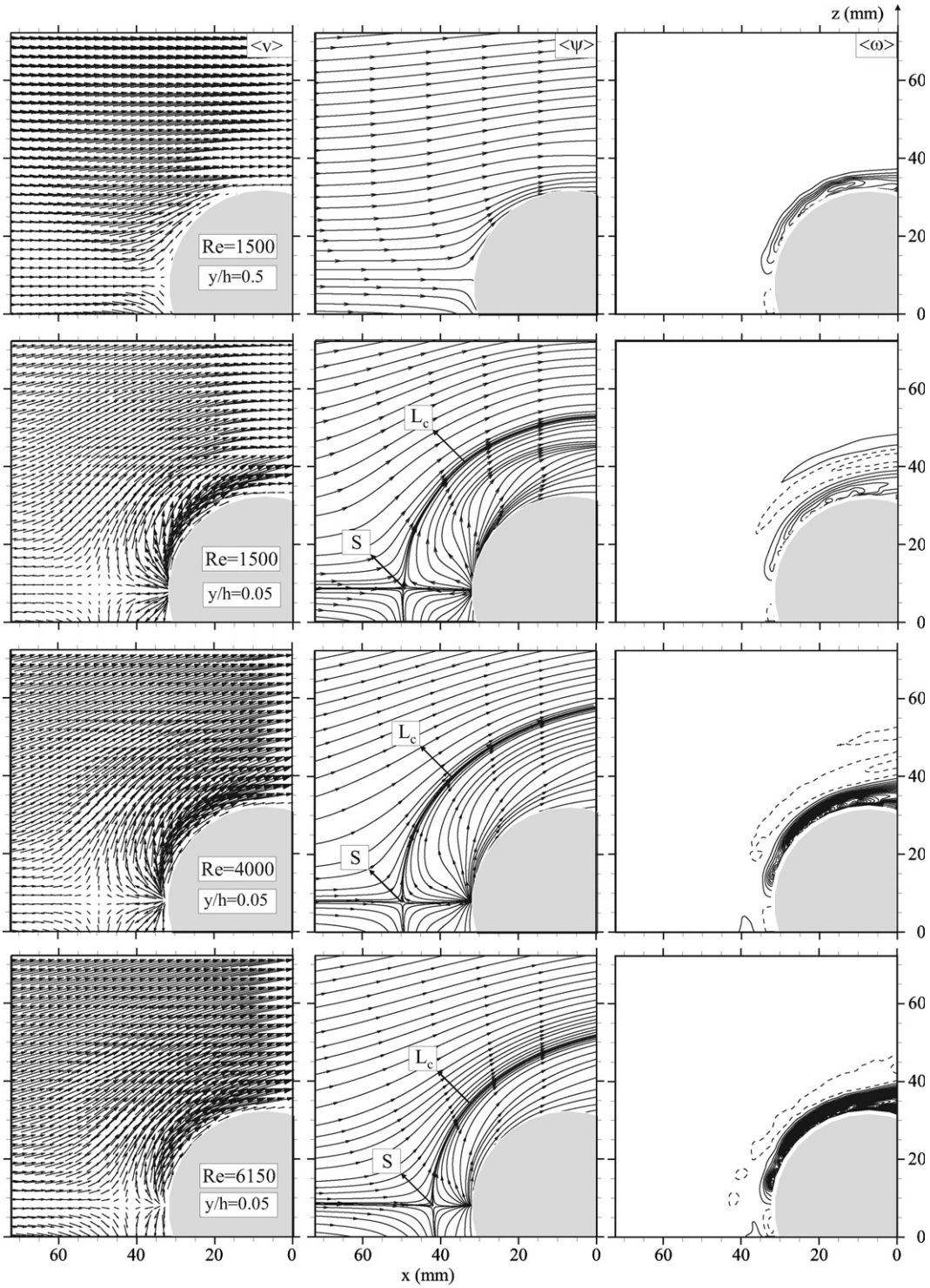

Fig. 2. Patterns of time-averaged velocity, $\langle V \rangle$, streamlines, $\langle \psi \rangle$ and vorticity, $\langle \omega \rangle$, minimum and incremental values of vorticity are $\langle \omega_{\min} \rangle = \pm 1\ s^{-1}$ and $\Delta \langle \omega \rangle = 2\ s^{-1}$.

system has a wide range of a coherent structures with a wide range of energetic frequencies in the velocity and pressure spectra when the approaching flow is turbulent. Time-averaged patterns of streamlines for both Reynolds numbers indicate the appearance of a saddle point, S_1 at the inner face of the shear layer close to the cylinder surface having a secondary focus, F_s upstream of this saddle point, S_1. On the center line of the wake flow, saddle point, S_2 is located upstream of the focus, F. Here, wake-flow region I which is surrounded by a secondary focus, F_s, saddle points, S_1, S_2 and Focus, F. This part of the wake-flow region does not receive fresh flow from the main (core) flow region as much as wake-flow region II situated downstream of the saddle point, S_2. In other words, wake-flow region II,

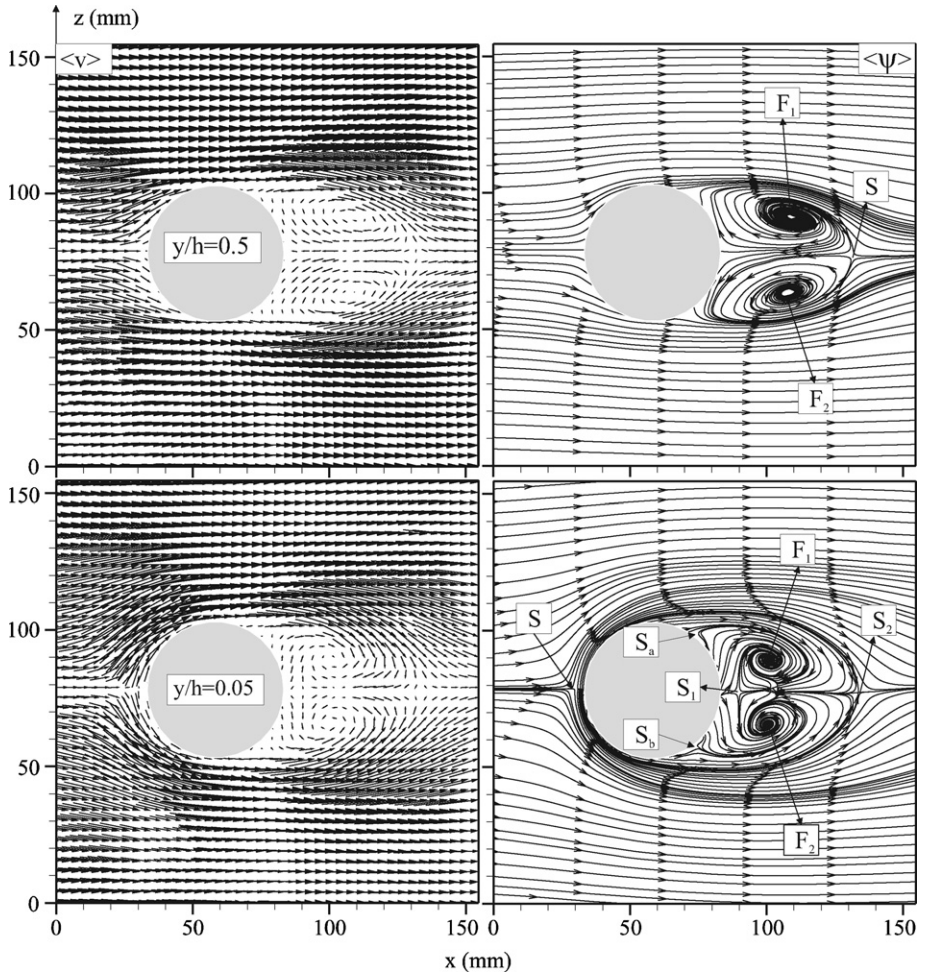

Fig. 3. Patterns of time-averaged velocity, $\langle V\rangle$, streamlines $\langle\psi\rangle$ and vorticity, $\langle\omega\rangle$, minimum and incremental values of vorticity are $\langle\omega_{\min}\rangle = \pm 1^{s-1}$ and $\Delta\langle\omega\rangle = 2^{s-1}$.

in between saddle points, S_1 and S_2, is exposed to a high rate of entrainment between the main (core) and wake-flow regions. Streamlines characterized by a line of coalescence, L_c, which passes through the saddle point, S located upstream of the cylinder base, reveal that the primary horseshoe vortex spirals inward towards the focus, F. Wake-region oriented streamlines, which occupy wake region I, reveal that there is a low level of entrainment between the main and the wake-flow regions. Distributions of the time-averaged velocity vectors, $\langle V\rangle$ and the corresponding patterns of streamlines, $\langle\psi\rangle$ clearly demonstrate that streamlines emerging from the upper face of the cylinder fed into focus, F. Fu and Rockwell (2005) concluded that an instability of the horseshoe vortices emerging upstream of the vertical cylinder activate the instability of the flow in the near wake. Upon increasing the Reynolds number of the flow, the saddle point, S_2 at the shoulder of the focus, F moves backward towards the cylinder surface. The animation of instantaneous flow data demonstrates that the saddle point, S_2 and focus, F travels forward and backward in the direction of the main flow. Along the shear layer, horseshoe vortex system takes place. Circulatory motions between wake and core flow regions are activated by this horseshoe vortex system emerging from the upstream side of the cylinder and these vortices migrate further downstream as illustrated by the images of the vorticity contours. Small positive and negative vortices occur close to the cylinder base at an elevation of $y/h = 0.05$ for all Reynolds numbers.

Distributions of the instantaneous velocity vector, V and corresponding patterns of streamlines, ψ at an elevation of $y/h = 0.05$ for $Re_d = 4000$ are presented in Fig. 5. Both instantaneous velocity vector distributions, nodes of attachment, and streamlines, ψ indicate that there are two saddle points, S_1, and S_2 and nodes of attachments, N_{a1} and N_{a2} on the upstream side of the cylinder. These saddle points appear just in front of the primary and developing horseshoe vortices. Through the animation of these instantaneous 490 images, it is observed that these points travel forward and backward in the main flow direction upstream of the cylinder. Fu and Rockwell (2005) obtained a similar result in shallow-water flow past a circular cylinder. Sahin et al. (2006) obtained three different saddle points located upstream of the cylinder in deep-water flow.

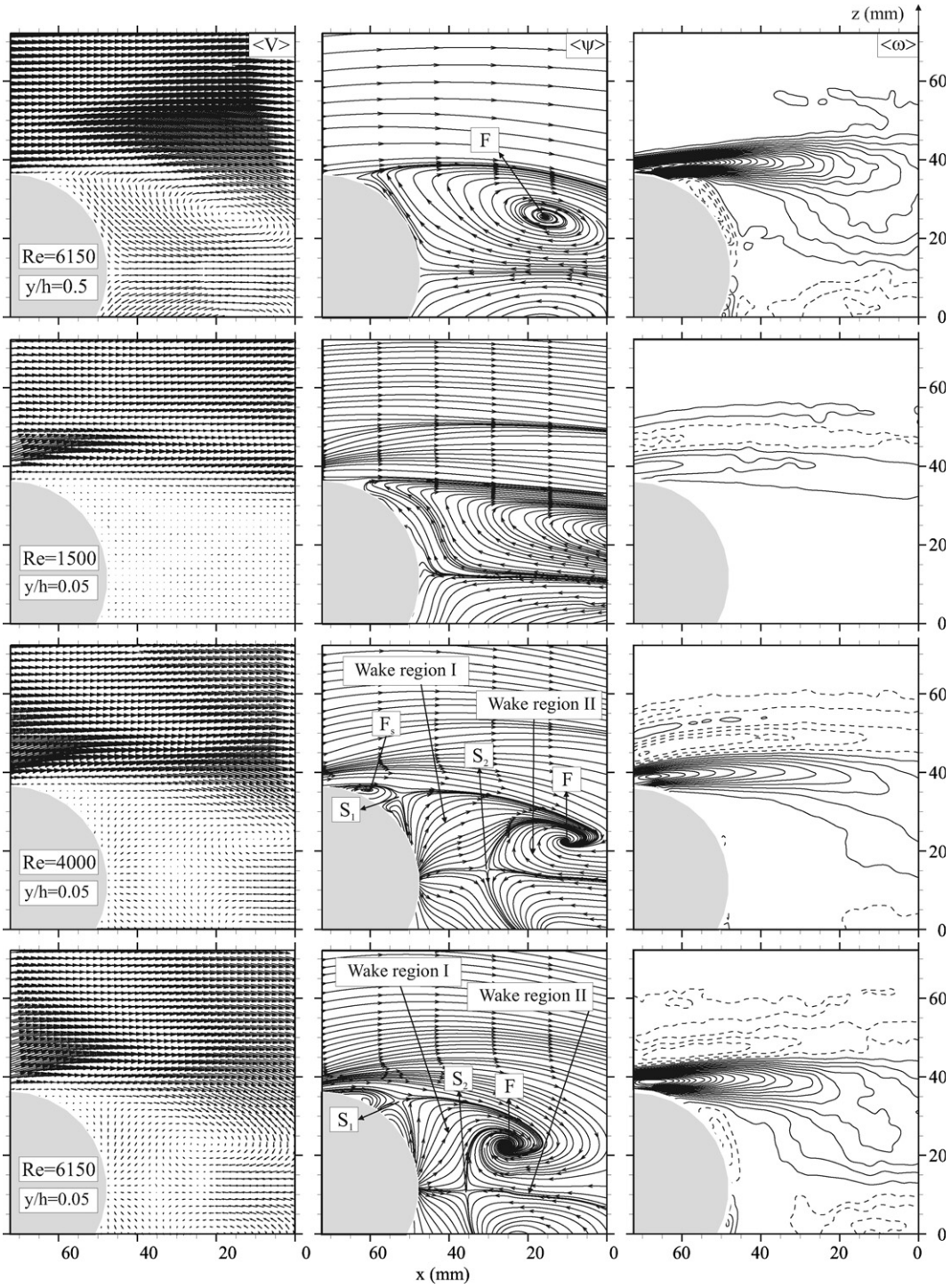

Fig. 4. Patterns of time-averaged velocity, $\langle V \rangle$ and streamlines, $\langle \psi \rangle$ for Reynolds number $Re_d = 6150$.

In the present studies, lines of convergence or coalescence, L_{c1} and L_{c2} pass through these saddle points, S_1 and S_2. These two vortices merge to combine and form primary horseshoe vortices in random motion.

As Marakkos and Turner (2006) have indicated, past experimental studies are limited because of the difficulties in measuring the unsteady flow data. For this reason, most of the past work on horseshoe vortex systems was qualitative using flow visualization point-wise measurement of time-averaged velocity information and velocity spectra. Nowadays particle image velocimetry gives an opportunity to the researcher to measure quantitatively the instantaneous velocity distribution across a defined flow field. In order to demonstrate the capability of the horseshoe type vortices, the formation, development of these vortices in the side-view plane, upstream of the cylinder, are presented

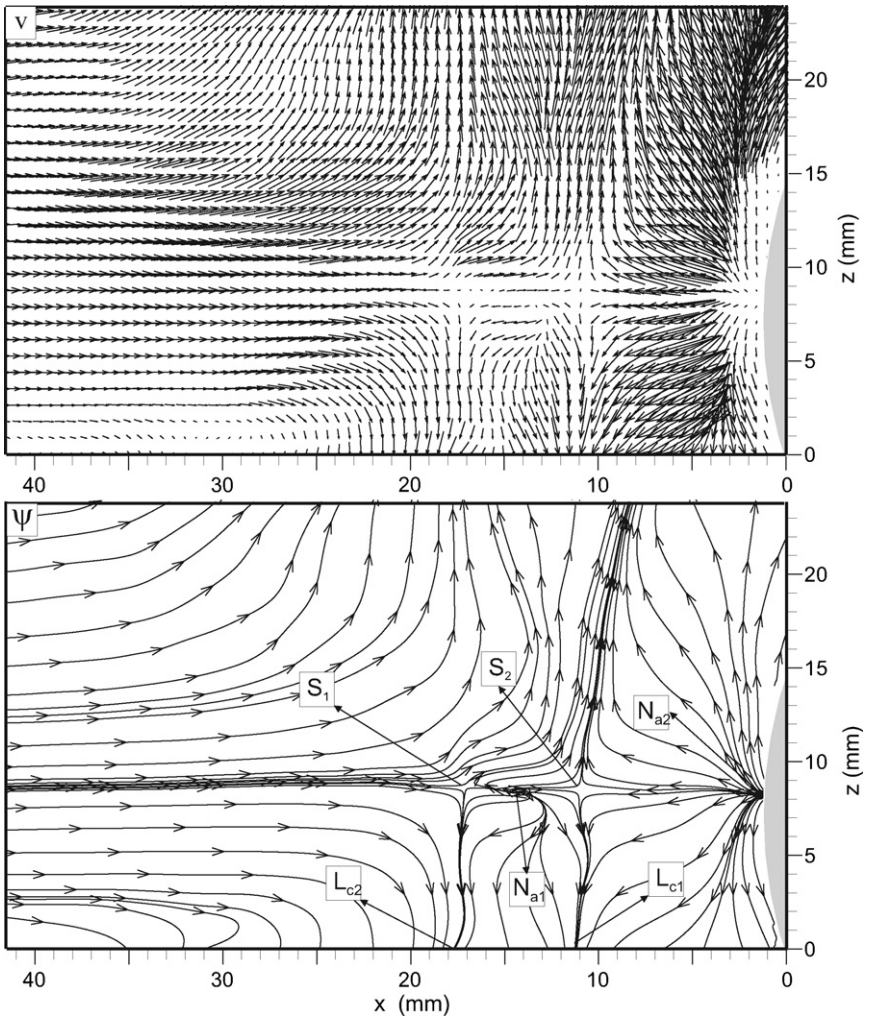

Fig. 5. Distributions of instantaneous velocity vector, V and patterns of streamlines, ψ in plan-view at $y/h = 0.1$ for $Re_d = 4000$.

in Fig. 6 for $Re_d = 4000$. Studies of the instantaneous flow data shows that multiple vortices are formed in the vicinity of the upper and lower plates. The instantaneous velocity vector, V and the corresponding patterns of streamlines, ψ for frame number $N = 66$ are shown in the first two images. A pair of Foci, F_1 and F_2, both having clock-wise rotation, and saddle points, S_1 and S_2 located in forward faces of Foci, F_1 and F_2 and counter-rotating vortex, V_c appear in between Foci, F_1 and F_2 in the vicinity of the lower plate. Identical flow characteristics are placed along the surface of the upper plate. Finally, a half-node of attachment, N_a, as referred to by Visbal (1991) and Khan and Ahmed (2005), are formed at the same position on both lower and upper plates. The distribution of the velocity vectors reveals virtually identical flow structures on both surfaces of the plates. For frame number $N = 331$ shown in the third and fourth images of Fig. 6, close to the lower plate, clock-wise rotating vortices occur and these are F, F_1, F_2 and F_3. As soon as a half-node of attachment point, N_a, appears focus F is formed which rolls up towards the plate-cylinder junction and gradually grows in size. It is worth mentioning that below each saddle point along the lower plate and above each saddle point along the upper plate, counter-rotating secondary vortices, V_c interact with the developing and primary vortices. These secondary vortices, V_c prevent merging of developing vortices with the primary vortices temporarily as observed in the animation of 490 instantaneous velocity vector fields and corresponding patterns of streamlines. Animation of these instantaneous flow data demonstrated that, as soon as these secondary or counter-rotating vortices, V_c disappear, the developing vortices combine with the primary vortices to form a large primary vortex which moves towards the plate-cylinder junction. The half-node of attachment point, N_a in frame, $N = 331$ on the lower plate surface is further away from the cylinder surface than the corresponding point, N_a close to the upper plate. Both instantaneous velocity vector maps, V and corresponding streamline patterns, ψ clearly indicate that the size of the recirculating flow region gradually increases as the flow moves towards the cylinder. The animation of 490 images also reveals that the vortical flow structure is sometimes dominant along the lower plate, while sometimes dominant along the upper plate. This is the reason that the starting points of the

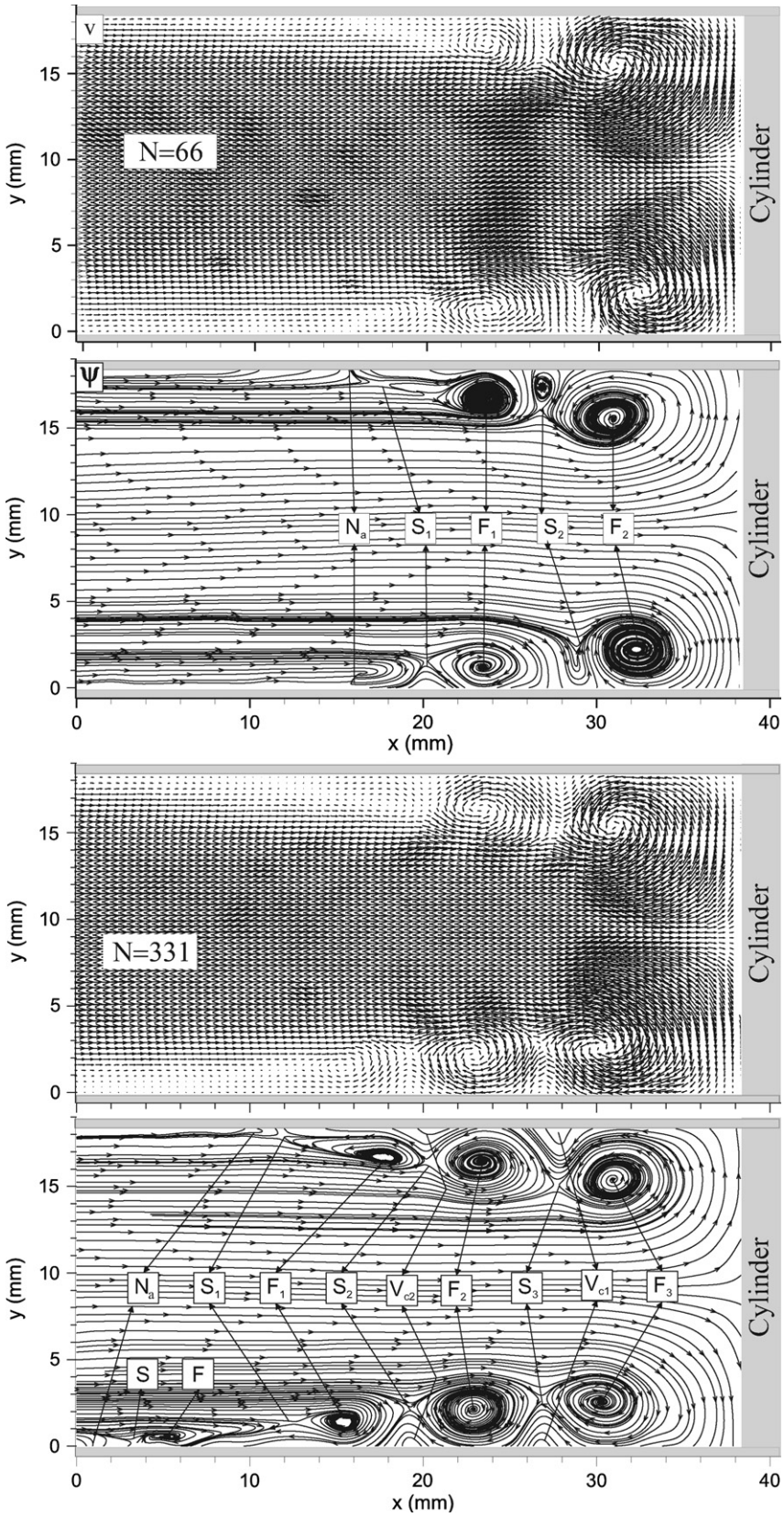

Fig. 6. Distributions of instantaneous velocity vector, V and patterns of streamlines, ψ in side-view in the upstream of the cylinder for $Re_d = 4000$.

recirculating flow region, (N_a) occur at different points on both surfaces of the plates for most of the time. It seems that it is necessary to conduct further quantitative experimental work in order to define the parameters which cause the instability and lead the vortical flow structure to become strongly unsteady. Numerical studies of Kirkil et al.

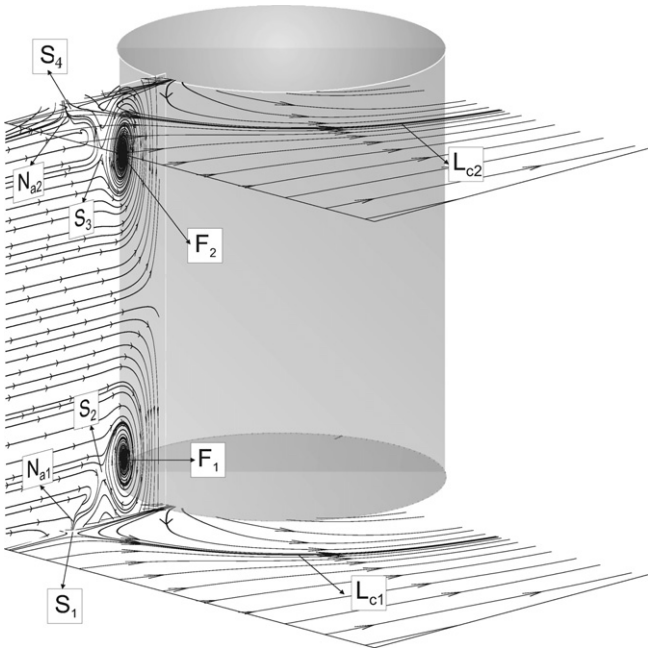

Fig. 7. Time-averaged patterns of streamlines, $\langle\psi\rangle$ in side-view and plane-view planes.

(2005) on the horseshoe vortex system around a cylinder bridge pier mounted on a flat bed reported that the secondary counter-rotating vortices at the floor interact very strongly with the developing and primary vortices which are also the case in the present studies. In general, separation occurs in both laminar and turbulent flow boundary layers, due to the streamwise adverse pressure gradient; but laminar boundary layers separate more easily than turbulent boundary layers. because, in the former, the increase of velocity with distance from the flat plate is less rapid, and the adverse pressure gradient can more readily halt the slow-moving fluid close to the plate surface. A turbulent boundary layer can resist this adverse pressure gradient for some distance further downstream before separating. That is why flow separation from the bottom surface appears to occur later at a higher value of Reynolds number. The narrow gap of the rectangular duct is one of the parameter which influences the vortical flow structure.

Patterns of time-averaged streamlines are shown in side-view and plan-view planes in Fig. 7 for the case of Reynolds number, $Re_d = 1500$. A pair of primary vortices, F_1 and F_2 accompanied by saddle points, S_2 and S_3 appears close to the lower and upper junctions. Half-nodes of attachment points, N_{a1} and N_{a2} occur close to the saddle points, S_2 and S_3. A half-node of attachment, N_{a1} coincides with the saddle point of S_1 on the lower plate and a half-node of attachment, N_{a2} coincides with the saddle point of S_4 on the surface of the upper plate as seen in Fig. 7.

4. Conclusions

Understanding the flow structure in the passage through a heat exchanger is vitally important for design and optimization purposes. In the past, most of research work was performed numerically due to difficulties of experimental studies in complex geometries (Tsai and Sheu, 1998). However, the vortical structure of the flow in the flow passage with two closely placed parallel plates with a built-in cylinder has been studied quantitatively using particle image velocimetry. Although the plates are closely spaced, a horseshoe vortex system appears along both sides of the plate surfaces. These vortices magnify the entrainment process which occurs between the main flow and the wake-flow regions and enhances the heat transfer rate. It has been realized that the rate of mixing gradually decreases, starting from the last saddle point downstream of the foci along a line towards the cylinder surface. Vortices in the reverse-flow region along both plate surfaces upstream of the cylinder rotate towards the cylinder as observed in the side-view planes. In between these rolling vortices a counter-rotating vortex attached to the surface of the plate occurs. These counter-rotating vortices gradually expand in size but lose strength and later disappear. As soon as these counter-rotating secondary vortices disappear, developing vortices in rolling motion combine together to form a primary vortex. Time-averaged and instantaneous flow data show that the entrainment process is increased between the main and wake-flow regions by the horseshoe vortex system hence leading to an enhancement of heat transfer rate in the case of fin-tube heat exchangers.

It is concluded that further quantitative experimental work should be performed in order to define the parameters which cause the instability and lead the vortical flow structure to become strongly unsteady.

Acknowledgements

The authors would like to acknowledge the financial support of the Office of Scientific Research Projects of Cukurova University for funding under contract nos: AAP20025 and MMF.2004.BAP.13.

References

Akilli, H., Rockwell, D., 2002. Vortex formation from a cylinder in shallow water. Physics of Fluids 14, 2957–2967.

Akkoca, A., 2004. Computational modeling of turbulent heat transfer in plate fin and tube heat exchangers. PhD thesis, Cukurova University, Institute of Natural and Applied Sciences, Department of Mechanical Engineering, Adana, Turkey.

Barsamian, H.R., Hassan, Y.A., 1997. Large Eddy simulation of turbulent cross flow in tube bundles. Nuclear Engineering and Design 172, 103–122.

Beale, S.B., Spalding, D.B., 1999. A numerical study of unsteady fluid flow in in-line and staggered tube banks. Journal of Fluids and Structures 13, 723–754.

Constantinescu, G., Koken, M., 2005. Time dependent and time averaged turbulence structure of flow past a surface mounted cylinder. In: Proceedings of 4th ICCHMT Paris, France.

Fu, H., Rockwell, D., 2005. Shallow flow past a cylinder: transition phenomena at low Reynolds number. Journal of Fluid Mechanics 540, 75–97.

Goldstein Jr., L., Sparrow, E.M., 1976. Experiments on the transfer characteristics of a corrugated fin and tube heat exchanger configuration. Journal of Heat Transfer, Trans ASME (February), 26–32.

Jang, J.Y., Chen, L.K., 1997. Numerical analysis of heat transfer and fluid flow in a three- dimensional wavy fin and tube heat exchanger. International Journal of Heat and Mass Transfer 40 (16), 3981–3990.

Jang, J.Y., Wu, M.C., Chang, W.J., 1996. Numerical and experimental studies of three- dimensional plate fin and tube heat exchangers. International Journal of Heat and Mass Transfer 39 (14), 3057–3066.

Kahraman, A., 2002. Investigation of flow structure from a vertical and horizontal cylinder in shallow water. PhD thesis, Cukurova University, Institute of Natural and Applied Sciences, Department of Mechanical Engineering, Adana, Turkey.

Khallaki, K., Russell, S., Baudoin, B., 2005. Numerical study of the horseshoe vortex structure upstream a single plate-finned tube. Heat and Technology 23 (1), 31–36.

Khan, M.J., Ahmed, A., 2005. Topological model of flow regimes in the plane of symmetry of a surface-mounted obstacle. Physics of Fluids 17 (1–8), 045101.

Kim, J.Y., Song, T.H., 2002. Microscopic phenomena and macroscopic evaluation of heat transfer from plate fins/circular tube assembly using naphthalene sublimation technique. International Journal of Heat and Mass Transfer 45, 3397–3404.

Kim, J.Y., Song, T.H., 2003. Effect of tube alignment on the heat/mass transfer from a plate fin and two-tube assembly: naphthalene sublimation results. International Journal of Heat and Mass Transfer 46, 3051–3059.

Kirkgoz, M.S., Ardiclioglu, M., 1997. Velocity profiles of developing and developed open channel flow. Journal of Hydraulic Engineering 123, 1099–1105.

Kirkil, G., Constantinescu, S.G. and Ettema, R. 2005. The horseshoe vortex system around a circular bridge pier on a flat bed. XXXIst International Association Hydraulic Research Congress, Seoul, Korea.

Kundu, D., Skeikh, A.H., Lou, D.Y.S., 1992. Heat transfer in cross flow over cylinders between two parallel plates. Numerical Heat Transfer, Part A 114, 558–564.

Lin, C., Chiu, P.H., Shieh, S.J., 2002. Characteristics of horseshoe vortex system near a vertical plate-base plate juncture. Experimental Thermal and Fluid Science 27, 25–46.

Marakkos, K., Turner, J.T., 2006. Vortex generation in the cross flow around a cylinder attached to an end-wall. Optics & Laser Technology 38, 277–285.

Mendez, R.R., Sen, M., Yang, K.T., Mcclain, R., 2000. Effect of fin spacing on convection in a plate fin and tube heat exchanger. International Journal of Heat and Mass Transfer 43, 39–51.

Ozturk, N.A., 2006. Investigation of flow characteristics in heat exchangers of various geometries. PhD thesis, Cukurova University, Institute of Natural and Applied Sciences, Department of Mechanical Engineering, Adana, Turkey.

Rocha, L.A.O., Saboya, F.E.M., Vargas, J.V.C., 1997. A comparative study of elliptical and circular sections in one- and two- row tubes and plate fin heat exchangers. International Journal of Heat and Fluid Flow 18, 247–252.

Roulund, A., Sumer, B.M., Fredsoe, J., Michelsen, J., 2005. Numerical and experimental investigation of flow and scour around a circular ple. Journal of Fluid Mechanics 534, 351–401.

Saboya, F.E.M., Sparrow, E.M., 1974. Local and average transfer coefficients for one row plate fin and tube heat exchanger configurations. Journal of Heat Transfer, Trans. ASME. (August), 265–272.

Sahin, B., Akkoca, A., Ozturk, N.A., Akilli, H., 2006. Investigation of flow characteristics in a plate fin and tube heat exchanger model composed of single cylinder. International Journal of Heat and Fluid Flow 27, 522–530.

Sarpkaya, T., 2004. A critical review of the intrinsic nature of vortex-induced vibrations. Journal of Fluids and Structures 18, 389–447.

Seal, C.V., Smith, C.R., Rockwell, D., 1997. Dynamics of the vorticity distribution in end-wall junctions. AIAA Journal 35, 1014–1047.

Sheui, T.W.H., Tsai, S.F., Chiang, T.P., 1999. Numerical study of heat transfer in two-row heat exchangers having extended fin surfaces. Numerical Heat Transfer, Part A: Applications 35, 797–814.

Simpson, R.L., 2001. Junction flows. Annual Review of Fluid Mechanics 33, 415–443.

Sumner, D., Price, S.J., Païdoussis, M.P., 1997. Investigation of impulsively-started flow around side-by-side circular cylinders: application of particle image velocimetry. Journal of Fluids and Structures 11, 597–615.

Tiwari, S., Biswas, G., Prasad, P.L.N., Basu, S., 2003. Numerical prediction of flow and heat transfer in a rectangular channel with a built-in circular tube. Journal of Heat Transfer 125, 413–421.

Torikoshi K., Xi G., Nakaszawa Y. and Asano H., 1994. Flow and heat transfer performance of a plat-fin and tube heat excahger, 1st report: Effect of fin pitch, in: Proceeding of the 10th International Heat Transfer conference, pp. 411–416.

Tsai, S.F., Sheu, T.W.H., 1998. Some physical insights into a two-row finned-tube heat transfer. Computers & Fluids 27, 29–46.

Tsai, S.F., Sheu, T.W.H., Lee, S.M., 1999. Heat transfer in a conjugate heat exchanger with a wavy fin surface. International Journal of Heat and Mass Transfer 42, 1735–1745.

Tutar, M., Akkoca, A., 2004. Numerical analysis of fluid flow and heat transfer characteristics in three-dimensional plate fin-and-tube heat exchangers. Numerical Heat Transfer; Part A: Applications 46, 301–321.

Umeda, S., Yang, W.-J., 1999. Interaction of Von Karman vortices and intersecting main streams in staggered tube bundles. Experiments in Fluids 26, 389–396.

Visbal, M.R., 1991. Structure of laminar juncture flows. AIAA Journal 29 (8), 1273–1282.

Westerweel, J., 1993. Digital particle image velocimetryTheory and Application. Delft University Press.

Westerweel, J., 1994. Efficient detection of spurious vectors in particle image velocimetry data sets. Experiments in Fluids 16, 236–247.

Wung, T.S., Chen, C.J., 1989. Finite analytic solution of convective heat transfer for tube arrays in cross flow: Part I – Flow field analysis. Journal of Heat Transfer 111 (August), 633–640.

Yuhi, M., Ishida, H., Umeda, S., 1999. A numerical study of sinusoidal oscillatory flows around a vertical wall-mounted circular cylinder. Coastal Engineering Journal 41 (3–4), 225–246.